


Article

# Design Contributions to the Elaboration of New Modeling Schemes for the Buckling Assessment of Hydraulic Actuators

Virgil Florescu <sup>1</sup>, Stefan Mocanu <sup>1</sup>, Laurențiu Rece <sup>1</sup>, Daniel Cătălin Motounu <sup>2</sup>, Aurel Gherghina <sup>3</sup> and Adrian Burlacu <sup>1,\*</sup> 

<sup>1</sup> Technical University of Civil Engineering of Bucharest, 020396 Bucharest, Romania; virgil.florescu@utcb.ro (V.F.); stefan.mocanu@utcb.ro (S.M.); rece@utcb.ro (L.R.)

<sup>2</sup> State Inspection for Control of Boilers, Pressure Vessels and Hoisting, 050524 Bucharest, Romania; daniel.motounu@gmail.com

<sup>3</sup> The Ministry of National Defense of Romania, 050561 Bucharest, Romania; stefan@lew.ro

\* Correspondence: adrian\_burlacu@yahoo.com; Tel.: +40-723-645-722

Received: 15 June 2020; Accepted: 14 August 2020; Published: 24 August 2020



**Abstract:** Hydraulic cylinders represent the main actuating/positioning element for standalone lifting equipment or equipment for various transport platforms. This type of actuator represents a structural component responsible for the operational safety of the equipment it serves. One of the most common and dangerous reasons concerning the end of life for this equipment is the buckling or loss of stability of the elastic equilibrium shape. This article aims to compare the classical approach of the problem in accordance with the strength of materials theory in relation to the numeric algorithms used in the applications for the analysis of structure behavior and the algorithms that are based on the finite element method. The subject of study is a hydraulic cylinder that is installed in a self-lifting platform and because of the manifestation of the phenomenon under analysis, it has led to a technical accident. For this purpose, an estimation of the value for the buckling critical load of the cylinder assembly was carried out.

**Keywords:** buckling; failure mode; elastic instability; critical force; buckling critical force; FEM (Finite Element Method)

## 1. Introduction

It is a fact that a structural element subjected to a central compression (axial) load will have the bearing capacity directly proportional with the minimum value of the axial moment of inertia relative to the axes of the reference system of the section. During the stages, this fact may show a tendency to create structures with significant slenderness-ratio factors, but these types of elements can become unstable because of the manifestation of the phenomenon of loss of stability of the elastic equilibrium shape, i.e., buckling [1–3].

Hydraulic cylinders are commonly mass-produced using traditional metals. High-strength steels are used for the production of the rod and the cylinder tube, whereas the pistons are generally made of aluminum. The core aspects of the hydraulic cylinder design are described by [4–6], whose manuals offer guidelines for designing such components effectively. These manuals present a complete scenario of problems and targets that need to be considered when designing the actuator, e.g., buckling analysis, strain and stress analyses, sealing performance and autofrettage investigations.

Buckling strength is a key component for hydraulic cylinders. Leonhard Euler's equation of buckling—as in elastic instability of structures—is still generally used in engineering practice. Euler's method is appropriate to analyze linearly elastic slender structures. However, it has demonstrated an

incapability to predict critical loads for structures of smaller slenderness with nonlinear behavior of material and imperfections of geometry and load [7].

In 2005, [8] assessed buckling instability by making an allowance for initial misalignment as an imperfection in the rod–cylinder tube intersection. The research defined the influence of the misalignment angle and friction coefficient on the buckling load by both numeric and experimental approaches.

Baragetti et al. [9,10] presented numeric models to analyze the buckling behavior of a double-acting cylinder. In the research, analytical and experimental models were used to study the influence of the friction coefficient, the geometric imperfections between the piston and rod–cylinder connections and the weight of the oil. A mathematical formulation, which accounts for the parameters previously introduced, was given and compared to experimental data. The pressure distribution acting on the wear rings was assumed in [10] to be triangular. This profile was probably suggested due to the fact that one of the sides of the seal is subject to zero pressure. However, the results of [11] show that the pressure profile along the contact zone remains fundamentally constant rather than triangular. In the case of rectangular seals with rounded edges, the pressure distribution exhibits lateral bumps for a frictionless contact whose values may be computed with the analytical approach presented in [12]. Therefore, the initial hypothesis of the pressure distribution considered between the seal and the piston-rod of a hydraulic actuator influences the wear of the seals and the leakage of the actuator.

In 2010, Morelli [13] presented experimental results on buckling occurrence for a telescopic actuator. Several pieces of research [14,15] studied stroke and cushioning devices to reduce the piston-rod kinetic energy during motion. They formulated a mathematical model of hydraulic circuits to study the supply pressure influence and alternative solutions were evaluated.

With respect to the material aspects, thin-walled composite cylinders have been researched for mechanical applications such as pressure vessels [16–19] and components that support energy absorption [20–23]. These components were gotten by filament winding, which is done by coupling an inner liner with an outer composite laminate.

The likelihood of using composite materials for hydraulic actuators seem to be inadequate; in fact, little contributions are evident [24–27]. In [24], the study presented an experimental test of hydraulic actuators on static and fatigue cyclic pressurization and, also other areas relating to wear. In [25,27], a methodology was presented for designing the cylinder tube and the rod in composites of a hydraulic actuator and the analytical results and the experimental data are compared. In [26], the feasibility of a hydraulic cylinder in composites is investigated by using numeric FEM analyses. Static analyses are exploited to examine the stress and the strain field caused by oil pressure. In addition, the buckling occurrence of the rod is analyzed. Optimization techniques have been applied to cylinder composite stacking sequence and shape in order to increase the critical buckling load. In [27], a hydraulic actuator made up of composites was applied to a telescopic hydraulic cylinder where the weight reduction obtained was approximately 96% compared to the cylinder in steel.

Recently, Fragassa et al. refer to the state of deformation occurred as a result of a given calculation scheme, the convergence of results being verified by means specific to resistive tensometry—the object of study is represented by the telescopic structure of the arm itself, focusing on areas of transition between sections (sliding pads). Measuring deformations were used to validate different design assumptions and to investigate the presence of local instability process, which is not predictable using only theoretical formulations [28].

In 2017, Pavlovic et al. dealt with the phenomenon of buckling at the global level of the telescopic arm of the machine, as a direct result of changing the geometric characteristics of the section of telescopic sections, by reducing the thickness of metal sheets, with direct implication on the stability of the structure itself. The paper highlighted the fact that the linear buckling techniques showed that critical loads and corresponding buckling modes were higher than the most extreme working conditions [29].

This paper aims to be a starting point in the approach—by means of the numeric algorithms based on the finite element method—of stability issues concerning slender structures subjected to axial compression. The high degree of complexity of the application demands a careful study with regard to the set of conditions initially established as input parameters.

The need to carry out this study is justified by the analysis of a technical accident caused by the manifestation of buckling failure of a hydraulic cylinder that is equipped in a self-lifting platform (Figure A1).

## 2. Materials

### 2.1. The Subject of the Study

The subject of the study is a GENIE Z135/70-TEREX hydraulic cylinder (Terex Corporation, Westport, CT, USA) installed on a self-lifting platform (Figures A2–A5) with the following main parameters:

- Maximum lifting load: 227.00 (kg);
- Working height: 43.15 (m),

The equipment provided with this cylinder was accompanied by a declaration of conformity according to the EC Directive 98/37/CE (Directive 98/37/EC of the European Parliament and of the Council of 22 June 1998 on the approximation of the laws of the member states relating to machinery; internal standards). The position in which the platform was found immediately after the accident is illustrated in Figures 1 and A6.



**Figure 1.** Position of the platform after the accident.

Following the visual examination, it was identified that the element that led to the collapse of the platform is the hydraulic cylinder that actuates the articulated arm, as shown in Figure 1. No other constructive elements of the platform with plastic deformations were identified; hence the collapse of the platform could be determined.

### 2.2. Laboratory Examinations of the Elements That Have Failed

#### 2.2.1. Macroscopic Analysis

In order to carry out the macroscopic analysis of the affected areas as a result of the mechanical failure of the construction elements of the equipment, the hydraulic cylinder of the platform was

disassembled and isolated. The images with the deformed element (the buckled element), collected samples, the state of the material in the contraction area and the stretched area are presented in Figures 2 and 3, respectively.

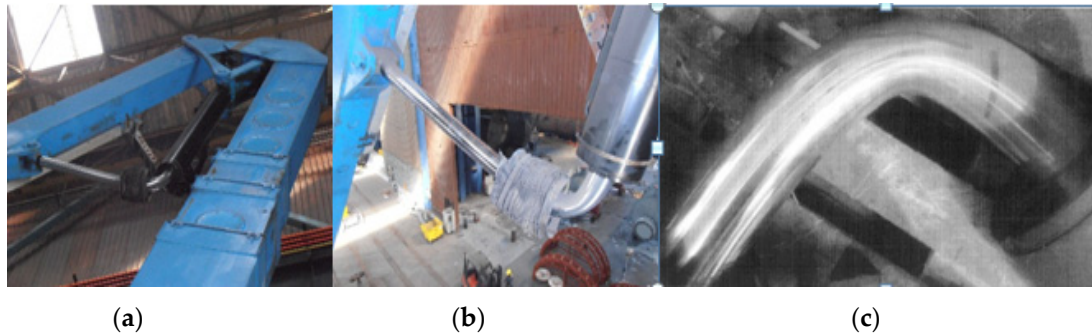


**Figure 2.** Buckled element. (a) General structure view; (b) actuator area; (c) actuator rod.

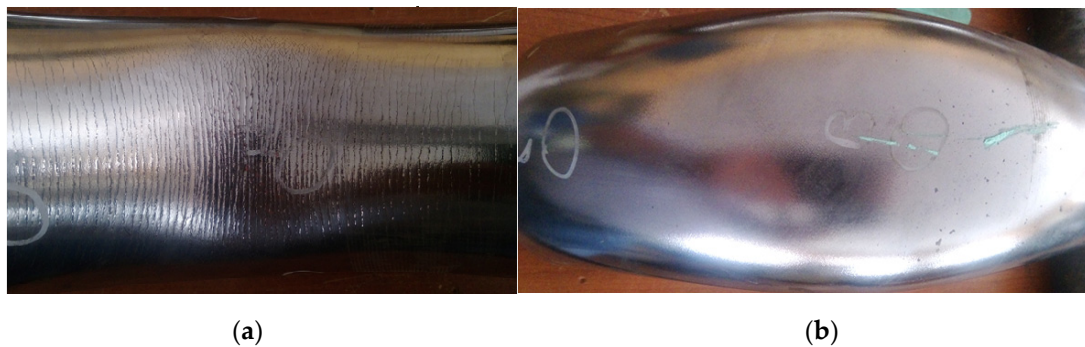


**Figure 3.** State of the material. (a) In the contraction area; (b) in the stretched area.

The exposed length of the actuator's rod in the position in which the accident occurred (Figure 3) is  $l = 1525.00$  mm.

The evaluation of the dimensional changes of the thickness of the elements that have yielded and the metallographic analysis of the materials from which the structures were made are presented in Figure 4.

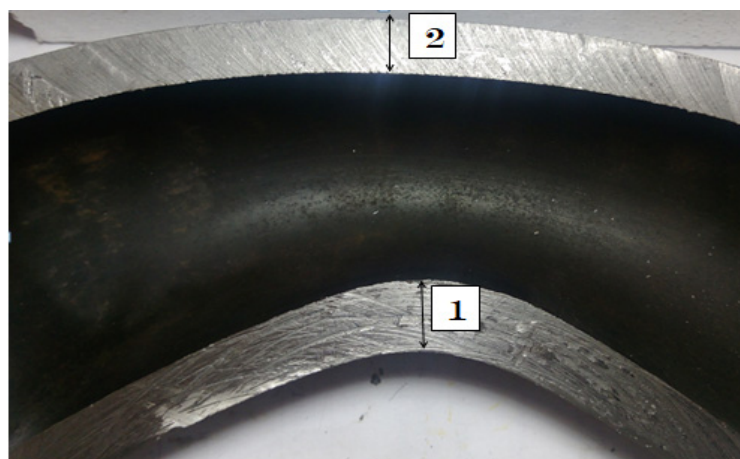


**Figure 4.** Section in the affected area: 1—maximum and 2—minimum thickness zones.

In the longitudinal section of the area affected by plastic deformation (Figure 4) and the buckling area, the maximum measured thickness is 11.60 mm (zone 1), and the minimum measured thickness is 8.30 mm (zone 2).

### 2.2.2. The Metallographic Analysis

In order to determine the material, samples were taken from both the affected and unaffected areas (numbered with 1 in Figure 5).



**Figure 5.** Collected samples from affected and unaffected areas of the rod.

Figure 6 illustrates structures corresponding both to the areas that were not affected and to the areas that have suffered plastic deformation.

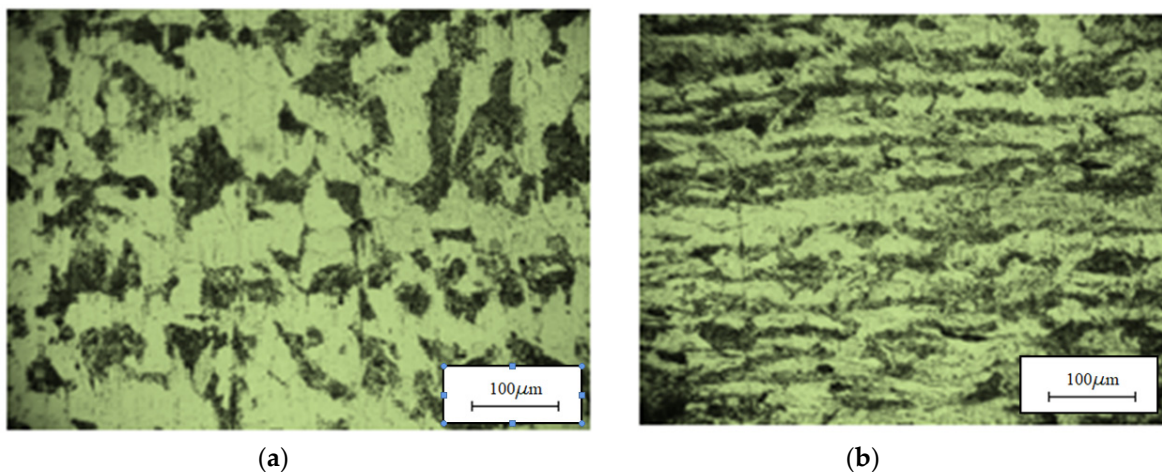


**Figure 6.** Metallographic structures. (a) With cold deformation; (b) with plastic deformation.

Figure 6b reveals structures characteristic of cold deformation, with different granular-dimensional parameters according to SR ISO 643/2013 between the stretched areas and the compressed areas (Figure 6a).

Table 1 shows the mechanical characteristics of the material from which the rod of the hydraulic actuator was made in accordance with the results of the metallographic analysis bulletin, the results of the traction test of a specimen taken from a non-deformed area of the rod of the piston (Position 1, Figure 5) and as well as the data obtained regarding the chemical structure of the material in accordance with the optical emission spectral analysis.

**Table 1a.** Chemical structure in weight%.

C	Si	Mn	P	S	Cu	Ni	Cr	Mo	V	Al
0.230	0.200	0.820	0.018	0.006	0.010	0.010	0.020	0.003	0.001	0.025

**Table 1b.** Mechanical characteristics.

Diameter (mm)	Section (mm <sup>2</sup> )	Yield Load, F <sub>c</sub> (N)	Yield Stress, R <sub>c</sub> (N/mm <sup>2</sup> )	Ultimate Fracture load, F <sub>m</sub> (N)	Ultimate Fracture Stress, R <sub>m</sub> (N/mm <sup>2</sup> )	Elongation, A (%)	Ductility, Z (%)
Ø 10	78.50	35,200	448.40	44,300	564.30	20.00	24.00

### 3. Studies, Analyses and Numeric Simulations

The study aims to assess the value of the buckling critical load of the rod of the hydraulic cylinder that was disassembled from the mobile platform following the accident caused by its severe plastic deformation, which resulted in the collapse of the whole structure.

Following the data obtained by direct examination from the site of the accident and the data provided by the metallographic analysis bulletin drawn up after the detailed analysis of the hydraulic actuator itself, the cross-section dimensions of the rod of the hydraulic equipment was established as input data for calculation (for the exposed area—Figure 5):

The outer diameter of the rod of the cylinder  $D = 94.50$  (mm)

The inner diameter of the rod of the cylinder  $d = 70.00$  (mm)

With the initial data presented above, one can calculate the slenderness ratio of the exposed segment of the rod, and its length is determined by the position of the structural system components at the time of the occurrence of the event (Figures 7 and 8, Figures A7–A10), as follows:

$$\left. \begin{aligned} A_{ef} &= \frac{\pi}{4}(94.5^2 - 70^2); A_{ef} = 3165 \text{ mm}^2, \\ I_{ax} &= \frac{\pi}{64}(94.5^4 - 70^4); I_{ax} = 2.736 \times 10^6 \text{ mm}^4, \\ i_{ef} &= \sqrt{\frac{2.736 \times 10^6}{3165}}; i_{ef} = 29.4 \text{ mm}, \end{aligned} \right\} \Rightarrow \lambda_{l_f=2l} = \frac{2 \times 1525}{29.4}; \lambda_{l_f=2l} = 103.7, \quad (1)$$

where:

$A_{ef}$  is the effective transversal cross section area;

$I_{ax}$  is the axial moment of inertia;

$i_{ef}$  the corresponding gyration radius;

$\lambda$  the slenderness coefficient.

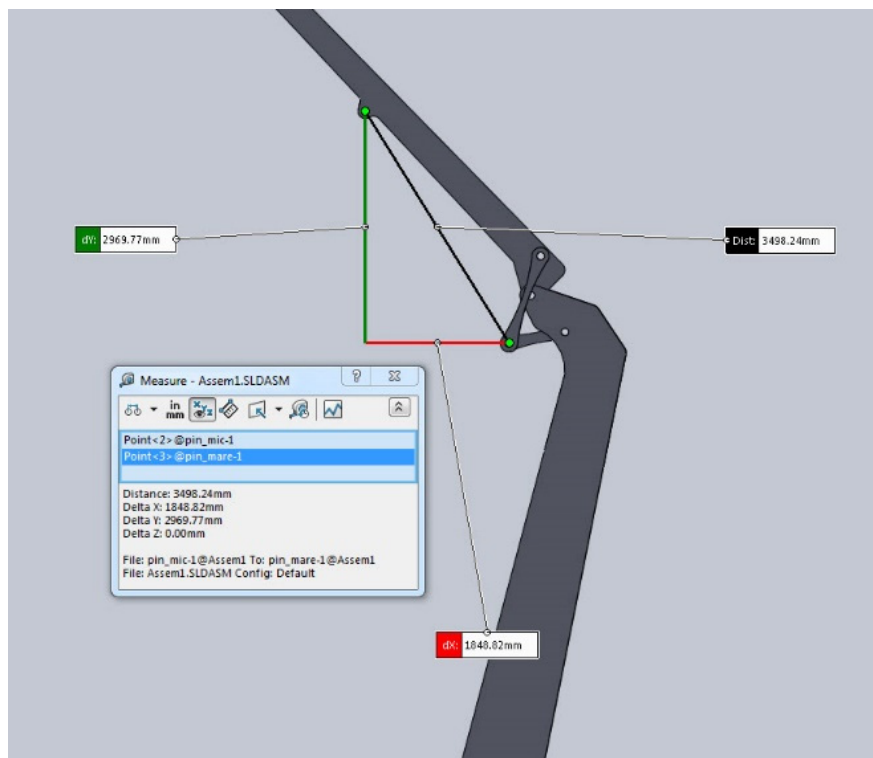


Figure 7. Actuator-rod parameters.

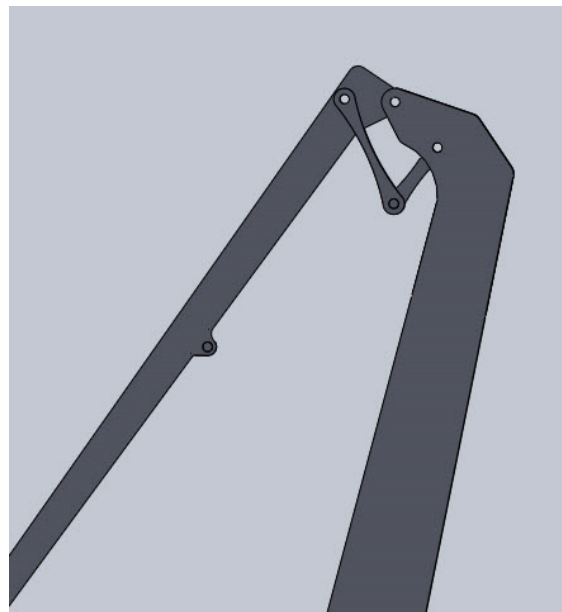


Figure 8. Detail of key position.

The elementary relations from the Strength of Materials were used [1–3].

To continue the demonstration, a first value of the critical buckling load can be expressed using the Euler relation  $\left(P_{cr} = \frac{\pi^2 \times E \times I_{min}}{l_f^2}\right)$  and the high value of the slenderness factor indicates, for a type of steel as the one analyzed, the elastic (Euler) buckling domain, thus [1–3]:  $P_{cr}^{Euler} = \frac{\pi^2 \times 2.1 \times 10^5 \times 2.736 \times 10^6}{(2 \times 1525)^2}$ ;  $P_{cr}^{Euler} = 609.6 \text{ kN}$ .

A second value for the estimation of the buckling critical load can be obtained starting from the Johnson relation (Johnson's Parabola—Figure 9), an algorithm by means of which the problem can be

approached, which has two advantages: the first one refers to the general validity of the scheme (either in the area of elastic buckling or in the area of post-elastic buckling). The second advantage refers to the possibility of avoiding the quasi-empirical approaches of the Tetmajer–Jasinski formula-style, which is a method that would imply, for example, the existence of three buckling domains (a method with cumbersome and uncertain resolution). Hence:

$$\begin{aligned} \sigma_{cr.}^{\text{Johnson}} &= 448.4 - \frac{448.4^2}{4 \times \pi^2 \times 2.1 \times 10^5} \times 103.72; & \sigma_{cr.}^{\text{Johnson}} &= 187.6 \text{ N/mm}^2, \\ P_{cr.}^{\text{Johnson}} &= 187.6 \times 3165; & P_{cr.}^{\text{Johnson}} &= 593.8 \text{ kN}. \end{aligned} \quad (2)$$

where:

$\sigma_{cr.}^{\text{Johnson}}$  is the failure/ultimate load stress, as computed by Johnson formula, and  $P_{cr.}^{\text{Johnson}}$  the corresponding failure/ultimate load.

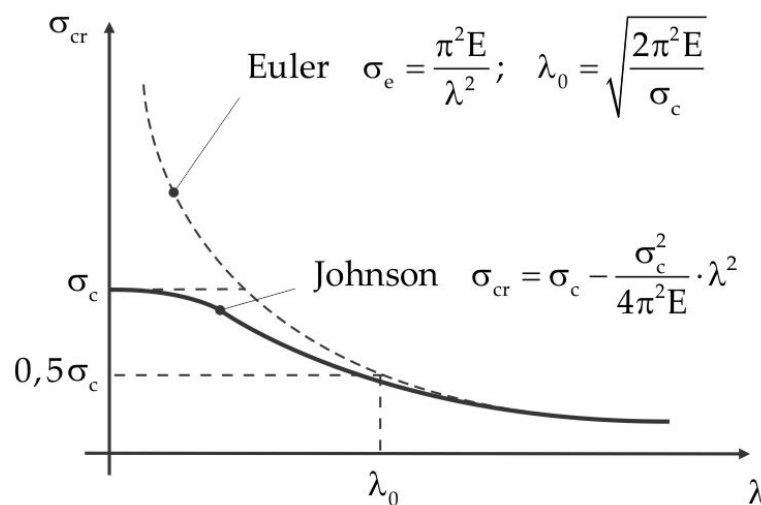


Figure 9. Johnson's Parabola.

In order to validate the results obtained by means of the classical analytical methods, it is necessary to model the behavior of the studied structure by the finite element method. The first stage of the modeling procedure implies the study of the hydraulic actuator's rod behavior (Figure 10); the study is divided into two parts. Part one implies an elastic buckling domain (Euler buckling) assessment, in order to verify the correctness for the used support scheme (Figures 11 and 12) on which the buckling length depends. Part 2 deals with a nonlinear analysis in order to establish the estimated value of the critical buckling load (Figure 13).

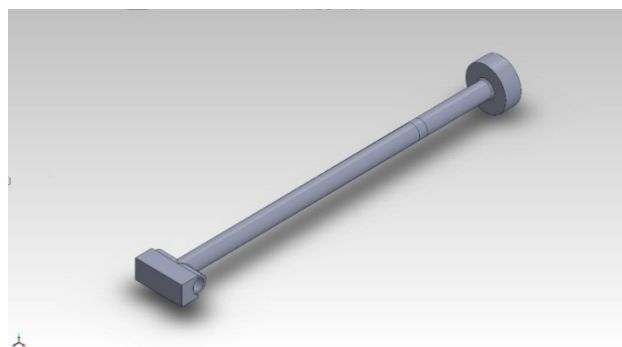
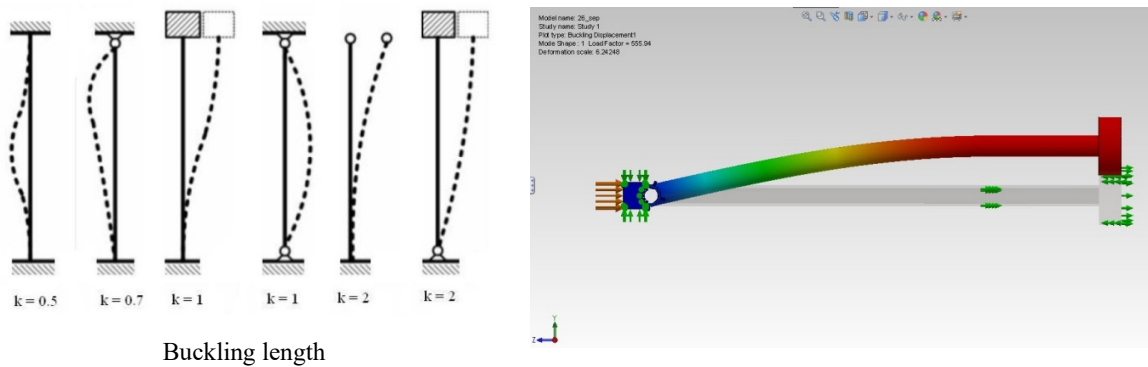


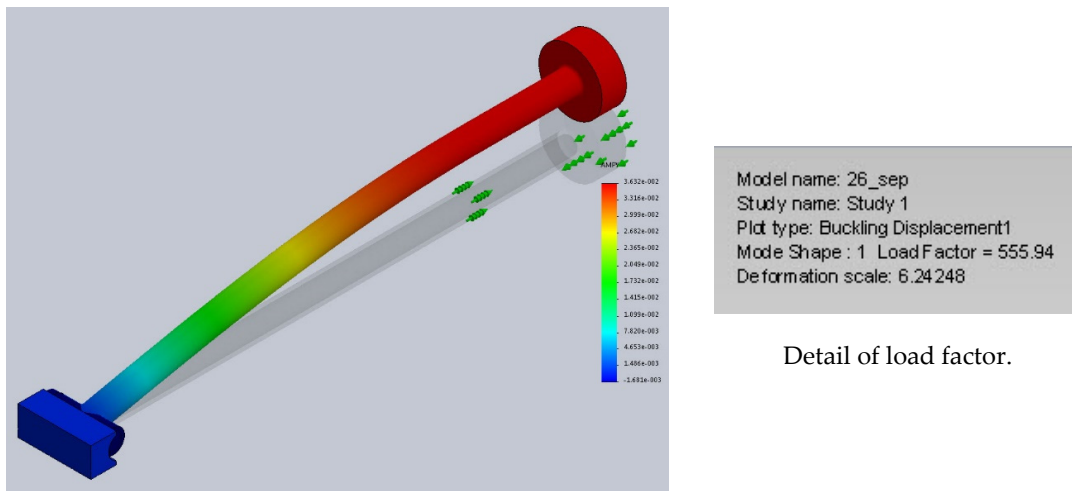
Figure 10. Hydraulic cylinder-rod solid model assembly, SolidWorks V 2014, Dassault Systèmes, Vélizy-Villacoublay, France.





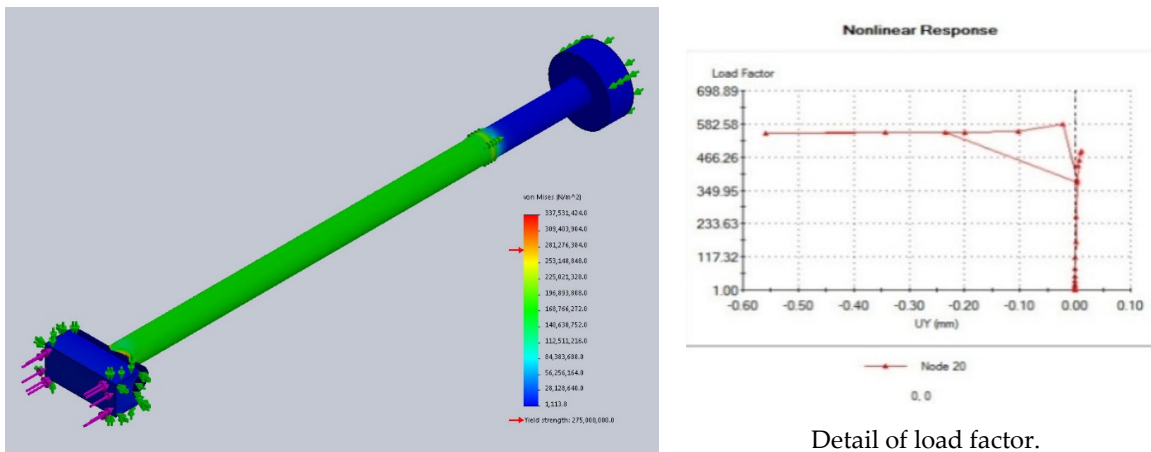
Buckling length

Figure 11. Deformed shape of the rod/buckling length output parameters.



Detail of load factor.

Figure 12. Buckling safety factor (load factor); Euler buckling output parameters.



Detail of load factor.

Figure 13. Buckling safety factor (load factor), nonlinear study output parameters.

In the second stage of modeling by means of the finite element method, the previous steps for the entire piston-rod-cylinder assembly of the studied element are followed (Figure 14) and the buckling study in the Euler domain validates the support scheme used (actuator articulated at both ends). This also indirectly confirms the hypothesis of a particular support scheme for the piston-rod-hinge/encastre with the possibility of translation (Figures 15 and 16).

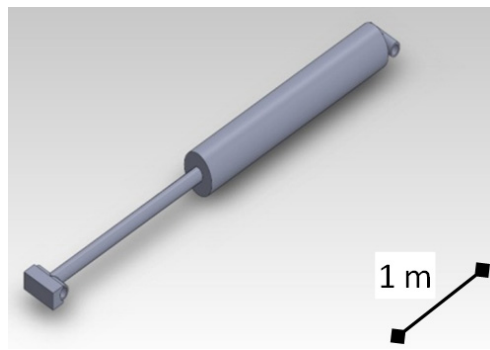


Figure 14. Piston rod–cylinder solid model assembly, SolidWorks 2014, Dassault Systèmes.

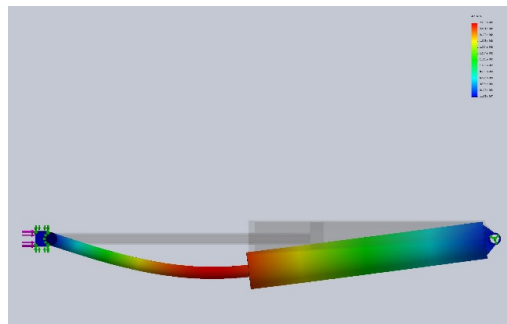


Figure 15. Deformed shape and buckling safety factor—output parameters.

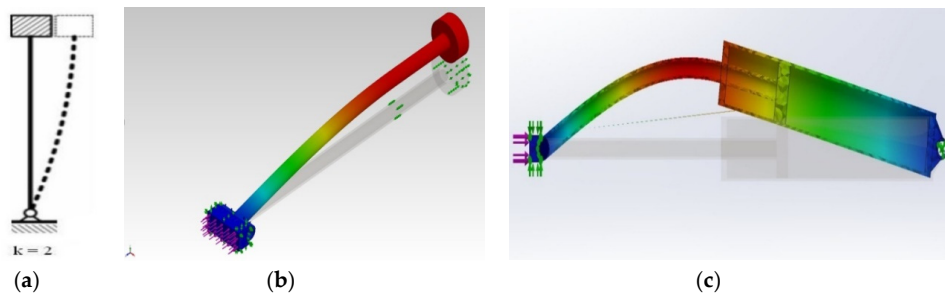


Figure 16. Computational scheme (a) and buckling length—input (b)/output (c) parameters.

#### 4. Results

The results of the nonlinear analysis for the piston–cylinder assembly are shown in Figure 17:

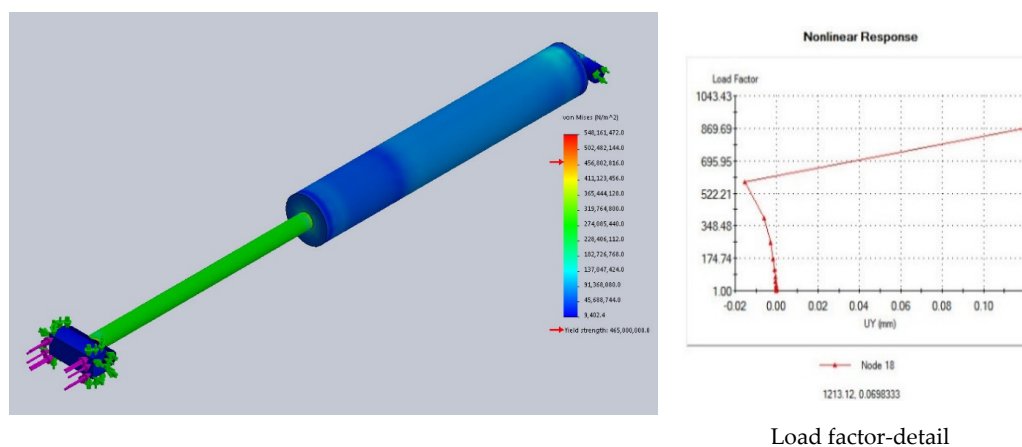


Figure 17. Buckling safety factor (load factor), the nonlinear study of the assembly—output parameters.

Regardless of the software application used, finding solutions to an analysis problem with the help of FEM involves solving several equations simultaneously, there are two major families of solving methods: the direct method, which uses numeric algorithms such as inverse matrix, LU decomposition, Gauss–Jordan, respectively iterative methods, in which approximate calculation techniques are used for finding a solution, the calculation sequence being repeated until the required degree of convergence is obtained.

In this case, we opt for the study with direct resolution algorithm DSS (direct sparse solver), given that the implicit iterative algorithms for solving FEPlus (finite-element plus), are more suitable for linear analysis.

After several simulation attempts, the maximum degree of accuracy of the solutions (including the absence of error messages) is obtained for the Crisfield–Riks control method for numeric simulation (incremental arc length control method), respectively for the Newton iterative calculation method—Raphson (NR) (Figure 18).

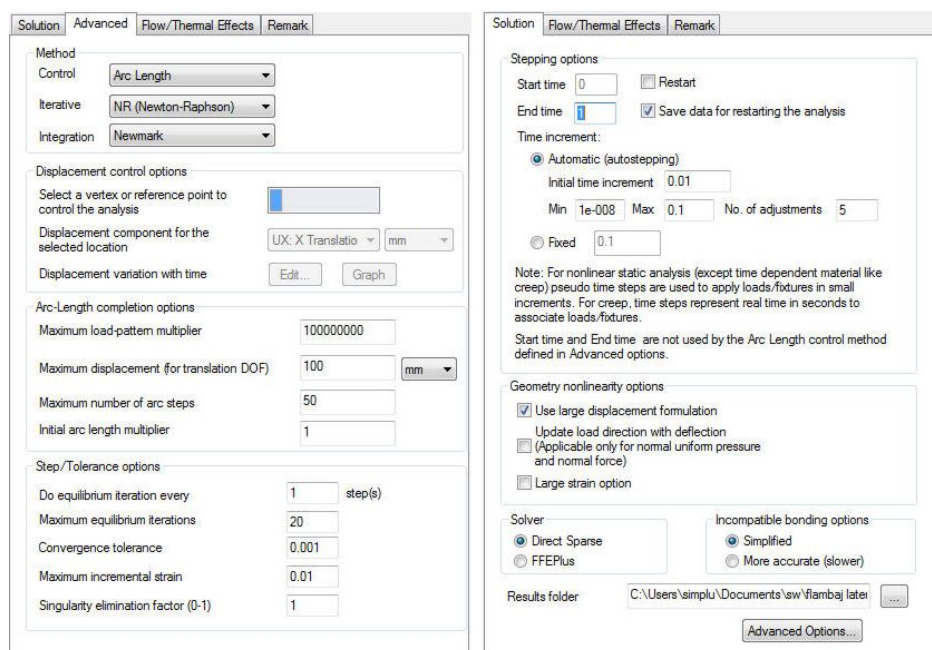


Figure 18. Nonlinear analysis settings.

In the case of nonlinear analysis, the system of equations to be solved at the generic moment  $t + \Delta t$ , is of the form:

$$\{R\}_{t+\Delta t} - \{F\}_{t+\Delta t} = 0, \quad (3)$$

where:

$R$  and  $F$  represents matrices of the vectors of the external loads applied in the nodes of the structure and, respectively matrices of the vectors of the internal efforts at the level of the nodes;

The need to use an iterative method is given by the dependence of the value of the matrix  $\{F\}_{t+\Delta t}$  on the matrix of the movements of the nodes of the network  $\{u\}_{t+\Delta t}$  at a given moment. Thus, the simplified form of a calculation step (rank  $i$  iteration) can be represented by the set of relations:

$$\begin{aligned} \{R\}_{t+\Delta t} - \{F\}_{t+\Delta t}^{(i-1)} &= \{\Delta R\}^{(i-1)}, \\ \{\Delta R\}^{(i-1)} &= [K]_{t+\Delta t}^{(i)} \{\Delta u\}^{(i)}, \\ \{\Delta u\}^{(i)} &= \{u\}_{t+\Delta t}^{(i)} - \{u\}_{t+\Delta t}^{(i-1)}, \\ \{u\}_{t+\Delta t}^0 &= \{u\}_t; \quad \{F\}_{t+\Delta t}^0 = \{F\}_t, \end{aligned} \quad (4)$$

where:

- $\{R\}_{t+\Delta t}$  the matrix of external loads at the level of the structure nodes;
- $\{F\}_{t+\Delta t}^{(i-1)}$  the matrix of internal efforts from the network nodes, at the iteration of rank “i”;
- $\{\Delta R\}^{(i-1)}$  the matrix of out-of-balance load vectors, at the iteration of rank “i”;
- $\{\Delta u\}^{(i)}$  the step matrix for displacements, at the iteration of rank “i”;
- $\{u\}_{t+\Delta t}^{(i)}$  displacement matrix, at the iteration of rank “i”;
- $[K]_{t+\Delta t}^{(i)}$  Jacobian matrix (tangent stiffness), l at the iteration of rank “i”.

The Newton–Raphson method of iterative calculation is represented schematically in Figure 19, in ordinate being represented the external loads and in abscissa the displacements; notice the reestimation of the Jacobian matrix terms for each iteration performed within the given calculation step ( $R_t \div R_{t+\Delta t} / u_t \div u_{t+\Delta t}$ ).

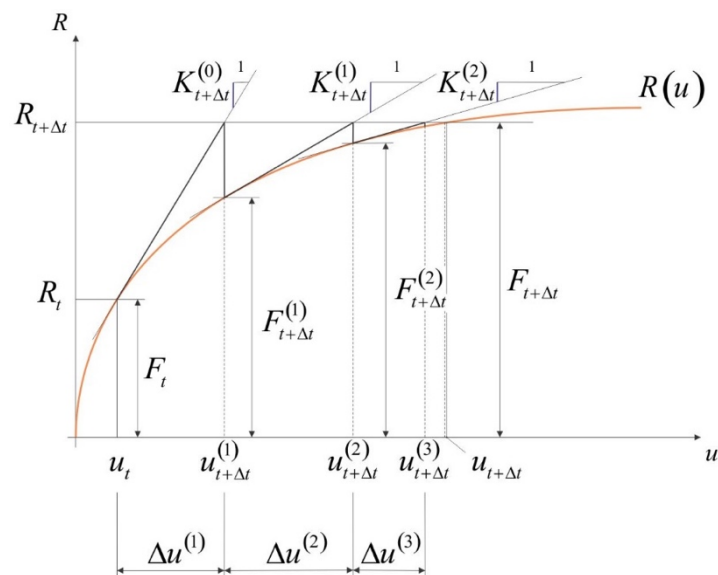


Figure 19. N–R method of iterative calculation.

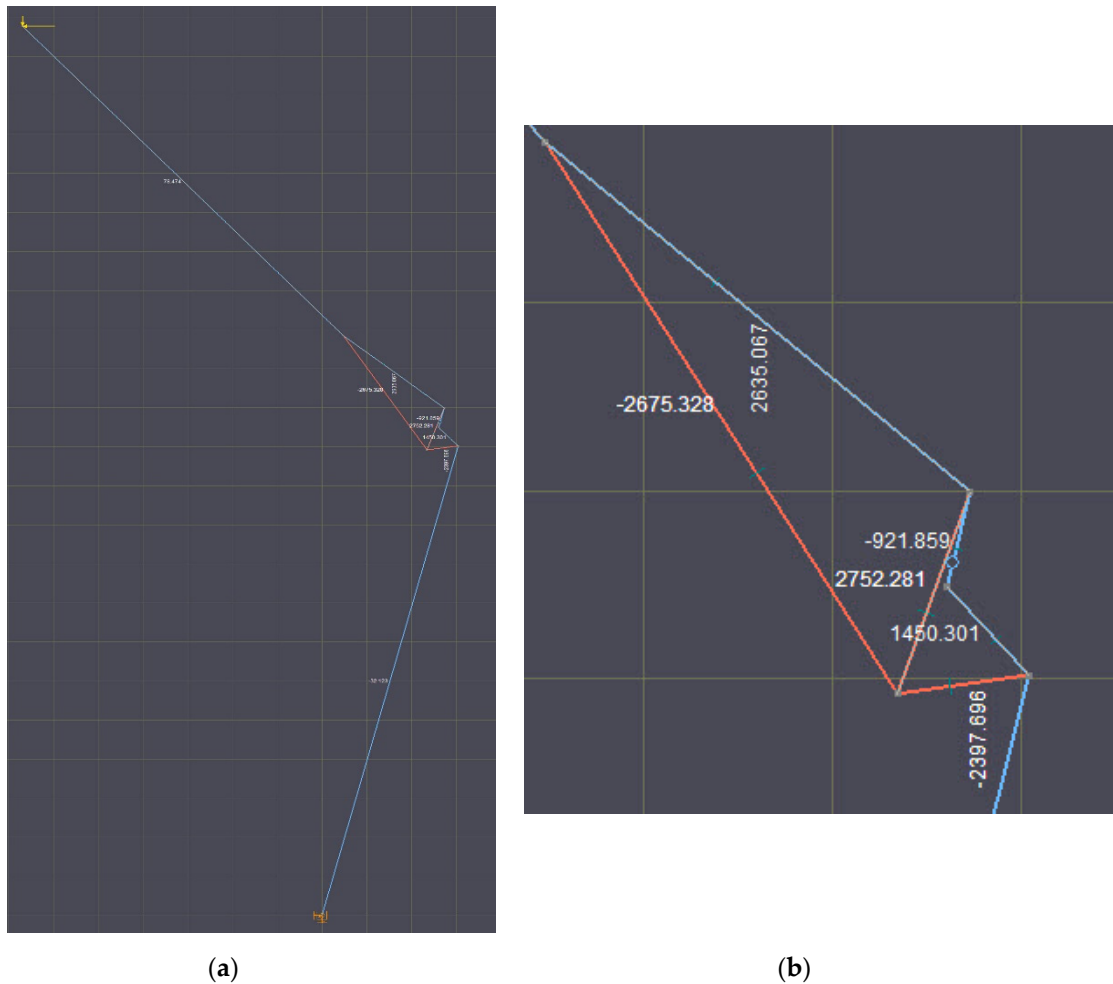
The use of the nonlinear solving algorithm is mainly due to the amplitude of the structural deformations, not being able to ignore the changes of the terms of the stiffness matrix with the increase of the load; in the case of state-of-the-art applications, the presence of a dedicated nonlinear calculation (large displacement formulation) option is noted, taking into account the large deformations of the studied structure, a variant valid when using solid meshing or shell discretization.

Table 2 below shows the comparative values of the study results, as follows:

Table 2. Values obtained by different methods.

Method Used	Critical Buckling Load (kN)	Hydraulic Fluid Pressure in the Cylinder Chamber (bar)
Euler	609.60	114.50
Johnson	593.80	111.51
Nonlinear modeling FEM—piston-rod	555.94	104.40
Nonlinear modeling FEM—piston-rod and cylinder assembly	586.99	110.24

By means of structural modeling at the main arm articulated structure level, one can see that the critical buckling load was exceeded several times in the circumstances in which the accident occurred; the loading scheme for this case study can only be presumed (Figures 20 and 21).



**Figure 20.** Beam internal forces/axial loads values. (a) Structure–beam internal forces; (b) detail of beam internal forces.

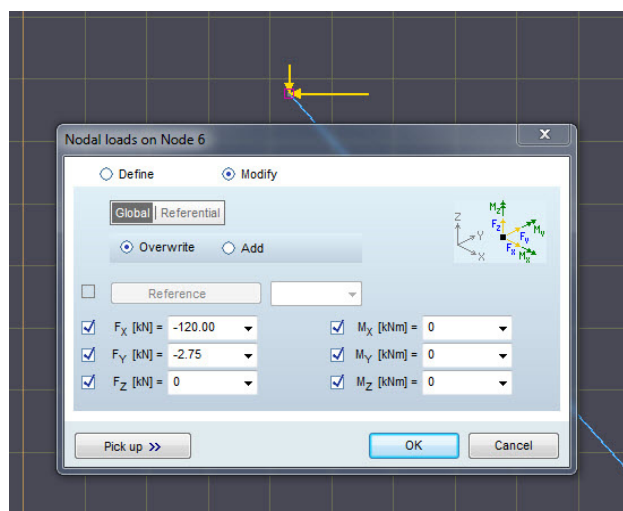


**Figure 21.** Boundary conditions for the loading scheme diagram—input parameters, AxisVM 9, InterCad, Budapest, Hungary.

## 5. Conclusions

The problem that led to the collapse of the articulated platform was the hydraulic device failure as a result of the occurrence of the buckling phenomenon for the mentioned rod.

Following the study, a certain degree of dispersion of the results has been noticed in the use of various software applications and working environment/working platforms used (Ansys, Solidworks for Windows, Salome-Mecca, OpenFoam, Code Aster for Linux). As a rule of thumb, at least two approaching methods should be used for comparison purposes.

For the studied case, the highest accuracy rank of the result (having referenced the traditional analytical solutions) was obtained for the latest generation of commercial software applications. Significant steps were made also for the open-source software with regard to the nonlinear analysis algorithms based on the finite element method. However, the lack of dedicated implementation programs (support schemes and complex loading schemes) and the lack of rich options in terms of solver settings were felt.

However, for the methodology applied in this article, it is worth noting the reduced spreading character of the estimated values for the critical buckling load, which confirms the validity of the obtained parameter and also the importance of support scheme modeling for the various cases considered, with direct implications on the accuracy of the output study parameters.

The article is limited to the detailed treatment of the phenomenon of loss of elastic equilibrium (buckling), at the level of the actuator rod that achieves the positioning of one of the component sections of the telescopic structure, a leading phenomenon to technical collapse from the general point of view of the structure. This approach is made starting from the behavior of the material from which the rod is made, with the mechanical properties and with the presented metallographic structure.

The occurrence of the undesirable phenomenon for the extension of the hydraulic actuator rod to a value lower than the maximum, with the inevitable displacement of the failure area by losing the elastic equilibrium from “Euler buckling” to the post-elastic or plastic buckling area, is due to the modification of the characteristic parameter “buckling length”, a parameter that depends on the effective support scheme of the rod at the moment of entry into operation of the studied failure mechanism.

Thus, the study showed a significant convergence of the results obtained in parallel with traditional calculation relations (giving up quasi-empirical calculation formulas of Tetmajer–Jasinski type in favor of the general Johnson relationship), respectively treatment by calculation with the finite element method (linear and nonlinear approach). The set of results naturally leads to the recommendation to modify the working parameters of the safety elements from the hydraulic actuation scheme of the hydraulic actuators in order to avoid reaching the working pressures that would generate the appearance of critical compression forces from the buckling phenomenon at the level of the actuating rod of the element in question. The convergence of the obtained solution is confirmed by the set of output parameters shown in Table 2, which thus validates the calculation methods studied.

**Author Contributions:** Conceptualization, V.F. and L.R.; methodology, V.F.; software, S.M.; validation, L.R., V.F.; formal analysis, S.M.; investigation, V.F., L.R., D.C.M. and A.G.; resources, A.B.; data curation, S.M., V.F.; writing—original draft preparation, V.F.; writing—review and editing, A.B.; visualization, S.M.; supervision, L.R. All authors have read and agreed to the published version of the manuscript.

**Funding:** This research received no external funding.

**Conflicts of Interest:** The authors declare no conflict of interest.

## Appendix A

Taking into account the fact that both calculation software solutions by the finite element method require modeling the structure without using any criteria of dimensional similarity (1:1 scale), establishing geometric parameters in terms of the calculation scheme used required the use of initial data obtained in situ (Figure A1). In addition, the data from the technical book, the user manual and the service maintenance log-data obtained from the manufacturer (Figures A2–A5) are presented.

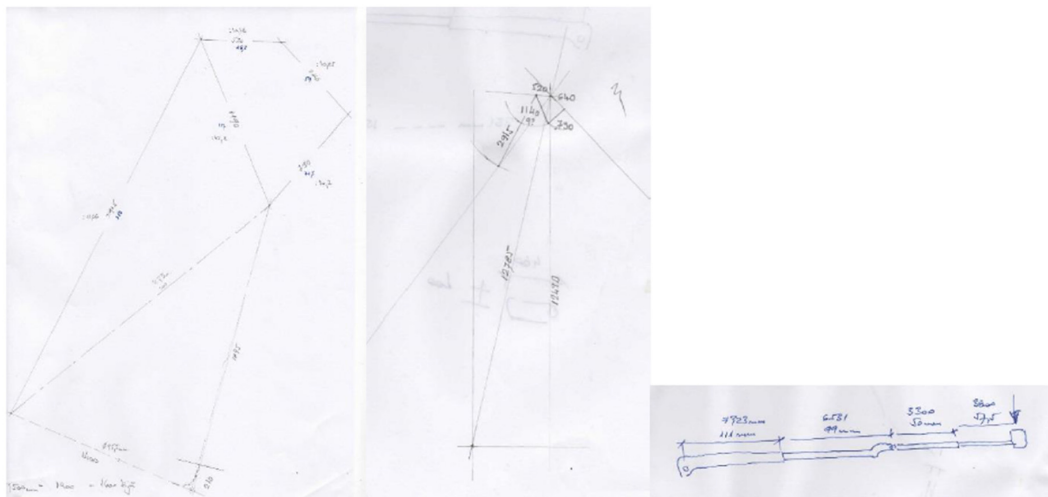


Figure A1. Initial in situ measurement data.

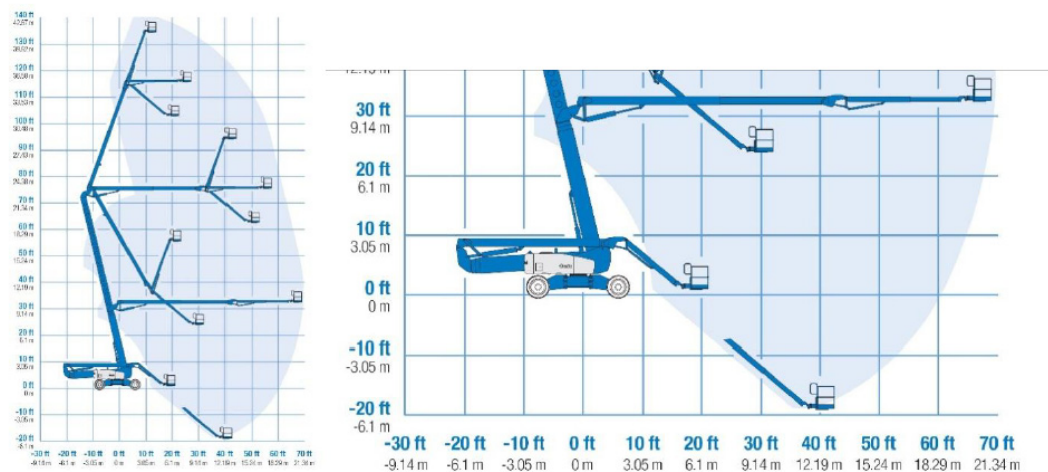


Figure A2. Boom geometrical data capabilities (according to manufacturer).

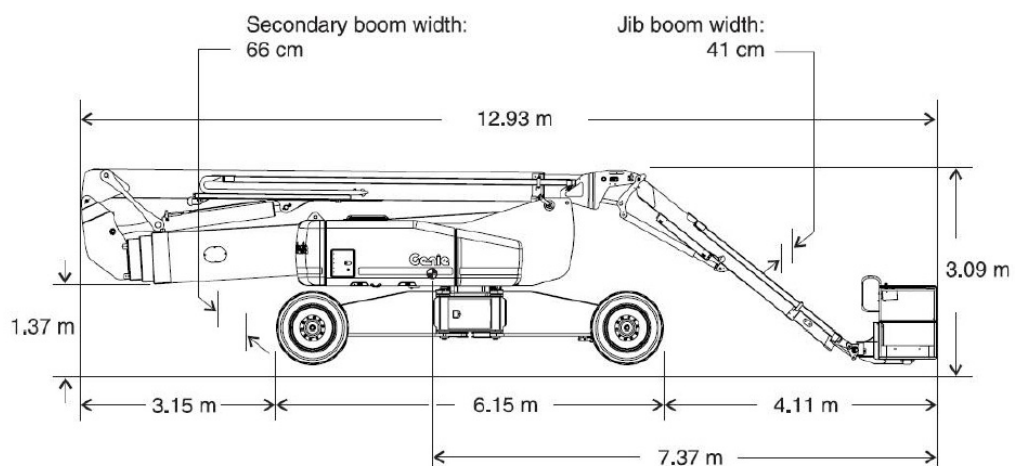


Figure A3. Parking geometrical data (according to manufacturer).

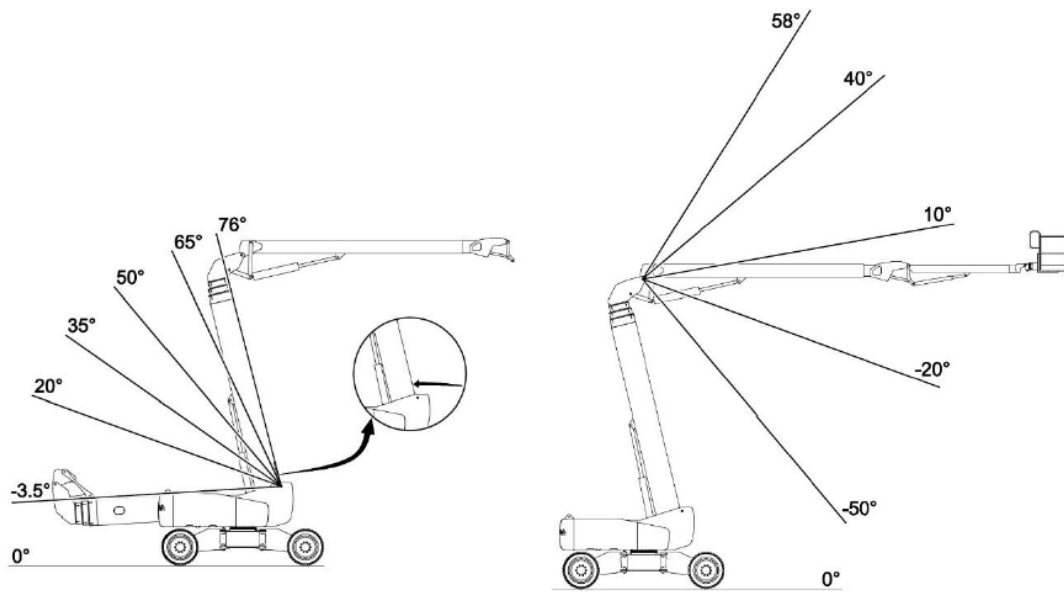


Figure A4. Primary and secondary boom array (according to manufacturer).

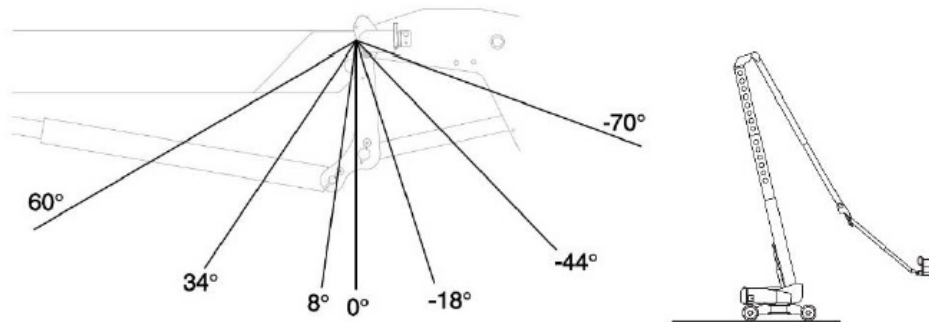


Figure A5. Actuator mechanism array (according to manufacturer).

After correlating the data thus obtained, we proceeded to model the structure, emphasizing the position in which the machine was found after consuming the event (Figures A6–A8).



(a)

Figure A6. Cont.





(b)

**Figure A6.** Position of the actuator mechanism after the accident (a) and the final position of the platform after the accident (b).

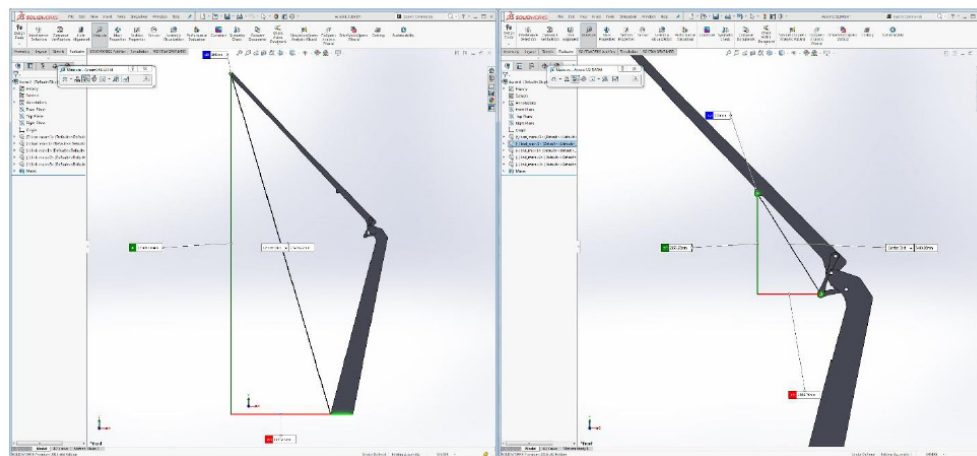


**Figure A7.** Geometrical data concerning the boom assemble and actuator mechanism respectively.

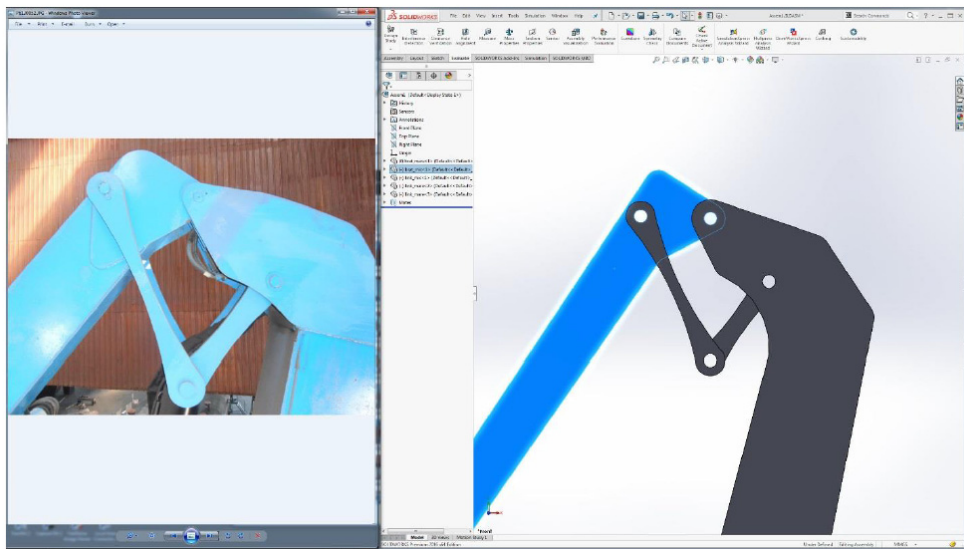


Figure A8. Detail of key position for actuator mechanism.

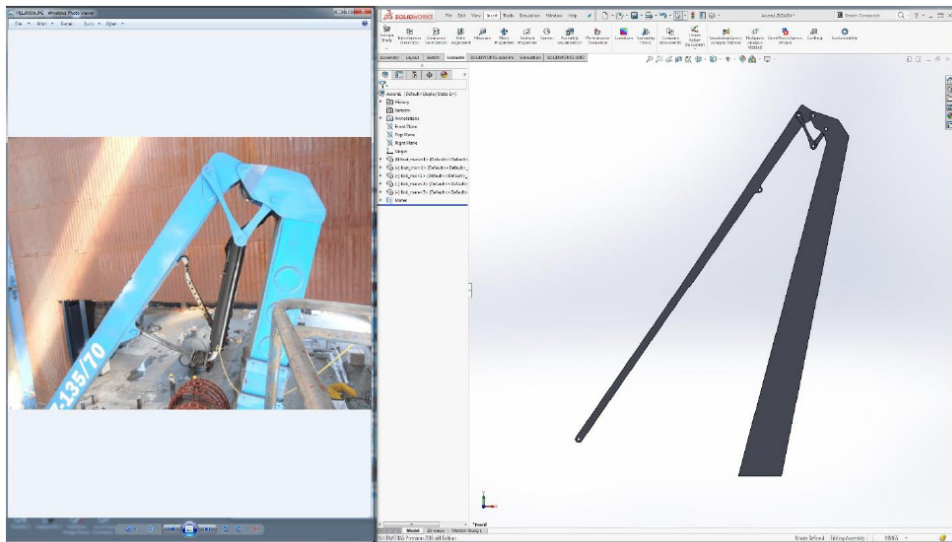


Figure A9. In situ versus kinematic numerical established data comparison.

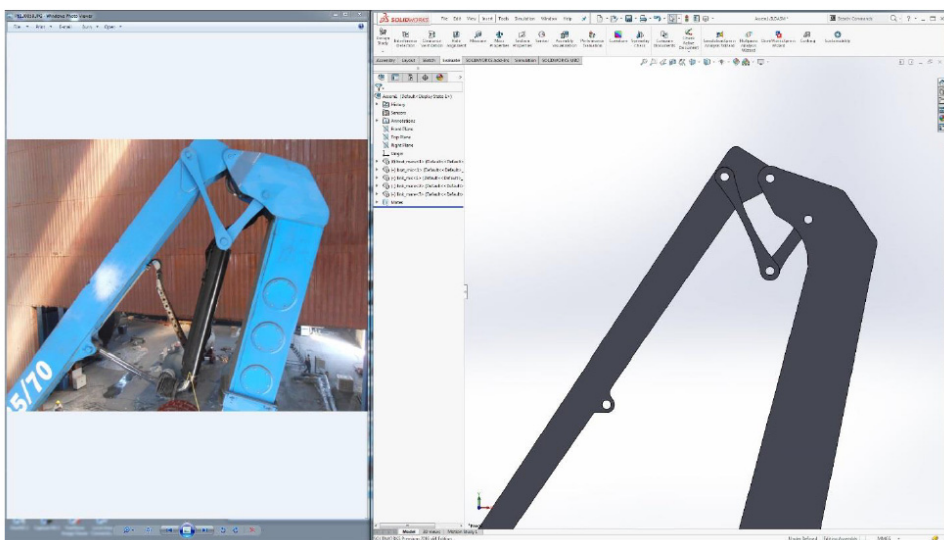


Figure A10. Actuator mechanism composing arms.

## References

1. Deutsch, I. *The Strength of Materials*; Didactic and Pedagogic Publishing House: Bucharest, Romania, 1979.
2. Ungureanu, I.; Ispas, B.; Constantinescu, E. *The Strength of Materials*; The Institute of Civil Engineering: Bucharest, Romania, 1981; Volume 2.
3. Andreescu, I.; Mocanu, Ş. *Compendium of the Strength of Materials*; Matrix Rom: Bucharest, Romania, 2005.
4. Hunt, T.; Vaughan, N. *The Hydraulic Handbook*, 9th ed.; Elsevier: Amsterdam, The Netherlands, 1996.
5. Speich, H.; Bucciarelli, A. *Manuale di Oleodinamica: Principi, Componenti, Circuiti, Applicazioni*; Tecniche Nuove: Milan, Italy, 2002.
6. Vullo, V. Circular cylinders and pressure vessels. In *Stress Analysis and Design*; Springer: Berlin/Heidelberg, Germany, 2014.
7. Evaldas, N. Buckling strength of hydraulic cylinders—An engineering approach and finite element analysis. *Mechanika* **2016**, *22*, 474–477.
8. Gamez-Montero, P.J.; Salazar, E.; Castilla, R.; Khamashta, M.; Codina, E. Misalignment effects on the load capacity of a hydraulic cylinder. *Int. J. Mech. Sci.* **2005**, *51*, 105–113. [[CrossRef](#)]
9. Baragetti, S.; Terranova, A. Bending behaviour of double-acting hydraulic actuator. *Proc. Inst. Mech. Eng. Part C J. Mech. Eng. Sci.* **2001**, *215*, 607–619. [[CrossRef](#)]
10. Baragetti, S.; Villa, F. Effects of geometrical clearances, supports friction, and wear rings on hydraulic actuators bending behavior. *Math. Probl. Eng.* **2016**. [[CrossRef](#)]
11. Field, G.J.; Nau, B.S. An experimental study of reciprocating rubber seals. In *Proceedings of the IMechE Symposium on Elastohydrodynamic Lubrication*; Institution of Mechanical Engineers: London, UK, 1972; pp. 29–36.
12. Strozzi, A.; Bertocchi, E.; Mantovani, S.; Giacomini, M.; Baldini, A. Analytical evaluation of the peak contact pressure in a rectangular elastomeric seal with rounded edges. *J. Strain Anal. Eng. Des.* **2016**, *51*, 304–317. [[CrossRef](#)]
13. Morelli, P. *On the Buckling Behaviour of Telescopic Hydraulic Cylinders, Key Engineering Materials*; Trans Tech Publications: Red Hook, NY, USA, 2010; Volume 417, pp. 281–284.
14. Lie, T.; Chapple, P.J.; Tilley, D.G. Actuator cushion performance simulation and test results. In *Proceedings of the Bath Workshop on Power Transmission and Motion Control (PTMC 2000)*, Bath, UK, 15–18 September 2000; pp. 187–198.
15. Schwartz, C.; De Negri, V.J.; Climaco, J.V. Modeling and analysis of an auto-adjustable stroke end cushioning device for hydraulic cylinders. *J. Braz. Soc. Mech. Sci. Eng.* **2005**, *27*, 415–425. [[CrossRef](#)]
16. Lifshitz, J.M.; Dayan, H. Filament-wound pressure vessel with thick metal liner. *Compos. Struct.* **1995**, *32*, 313–323. [[CrossRef](#)]
17. Chapelle, D.; Perreux, D. Optimal design of type 3 hydrogen vessel: Part I—Analytic modelling of the cylindrical section. *Int. J. Hydrogen Energy* **2006**, *31*, 627–638. [[CrossRef](#)]
18. Comond, C.; Perreux, D.; Thiebaud, F.; Weber, M. Methodology to improve the lifetime of type III HP tank with a steel liner. *Int. J. Hydrogen Energy* **2009**, *34*, 3077–3090. [[CrossRef](#)]
19. Gay, D.; Hoa, S.V.; Tsai, S.W. *Composite Materials: Design and Applications*, 3rd ed.; CRC Press: Boca Raton, FL, USA, 2015.
20. Bragohain, M.K. *Composite Structures Design, Mechanics, Analysis, Manufacturing and Testing*; CRC Press: Boca Raton, FL, USA, 2017.
21. Thesken, C.; Murthy, P.L.N.; Phoenix, S.L.; Greene, N.; Palko, J.L.; Eldridge, J.; Sutter, J.; Saulsberry, R.; Beeson, H. A Theoretical Investigation of Composite Overwrapped Pressure Vessel (COPV) Mechanics Applied to NASA Full-Scale Tests. Technical Memorandum. 2009. Available online: <https://ntrs.nasa.gov/citations/20090037028> (accessed on 8 April 2020).
22. Lanzi, L.; Castelletti, L.M.L.; Anghileri, M. Multi-objective optimization of composite absorber shape under crashworthiness requirements. *Compos. Struct.* **2004**, *65*, 433–441. [[CrossRef](#)]
23. Bisagni, C.; Di Pietro, G.; Frascini, L.; Terletti, D. Progressive crushing of fiber-reinforced composite structural components of a Formula One racing car. *Compos. Struct.* **2005**, *68*, 491–503. [[CrossRef](#)]
24. Otte, B.; Stelling, O.; Müller, C. High-Pressure Lightweight Hydraulic Fully Composite Piston Accumulators. In *Proceedings of the 8th International Fluid Power Conference*, Dresden, Germany, 26–28 March 2012.

25. Solazzi, L. Feasibility study of hydraulic cylinder subject to high pressure made of aluminum alloy and composite material. *Compos. Struct.* **2019**, *209*, 739–746. [[CrossRef](#)]
26. Solazzi, L. Design and experimental tests on hydraulic actuator made of composite material. *Compos. Struct.* **2020**, *232*. [[CrossRef](#)]
27. Solazzi, L.; Bunoli, A. Telescopic Hydraulic Cylinder Made of Composite Material. *Appl. Compos. Mater.* **2019**, *26*, 1189–1206. [[CrossRef](#)]
28. Fragassa, C.; Minak, G.; Pavlovic, A. Measuring deformations in the telescopic boom under static and dynamic load conditions. *Facta Univ. Ser. Mech. Eng.* **2020**, *18*, 315–328. [[CrossRef](#)]
29. Pavlovic, A.; Fragassa, C.; Minak, G. Buckling analysis of telescopic boom: Theoretical and numerical verification of sliding pads. *Tehnički Vjesnik* **2017**, *24*, 729–735. [[CrossRef](#)]



© 2020 by the authors. Licensee MDPI, Basel, Switzerland. This article is an open access article distributed under the terms and conditions of the Creative Commons Attribution (CC BY) license (<http://creativecommons.org/licenses/by/4.0/>).